Meccanica (2015) 50:1481–1494
DOI 10.1007/s11012-015-0100-9

Three-dimensional suction flow control and suction jet length optimization of NACA 0012 wing

Kianoosh Yousefi · Reza Saleh

Received: 8 December 2013 / Accepted: 8 January 2015 / Published online: 23 January 2015

Abstract A three-dimensional suction flow control study was performed to investigate the aerodynamic characteristics of a rectangular wing with a NACA 0012 airfoil section. In addition, the optimum suction jet length was determined. In this study, the Reynolds-averaged Navier–Stokes equations were employed in conjunction with a k–ω SST turbulent model. Perpendicular suction was applied at the leading edge of the wing's upper surface, with two different types of slot distributions: i.e., center suction and tip suction. The suction jet lengths were varied by 0.25–2 of the chord length, and the jet velocity was selected to be 0.5 times the freestream velocity. Most importantly, in both cases, the results indicated that the lift-to-drag ratio increased as the suction jet length rose. However, the improvement in aerodynamic characteristics was more pronounced with center suction, and these characteristics were extremely close to those of the case considering suction over the entire wing such that the jet length was equal to wingspan. Moreover, in the center suction case, vortexes frequently abated or moved downstream. Interestingly, under similar conditions, a greater number of vortexes were removed with center suction than with tip suction. Ultimately, when the jet length is less than half the wingspan, tip suction is the better of the two alternatives, and when the jet length is greater than half the wingspan, center suction is better suited.

Keywords 3D simulation · NACA 0012 wing · Flow control · Suction · Jet length

K. Yousefi (✉) · R. Saleh
Department of Mechanical Engineering, Mashhad Branch, Islamic Azad University, Mashhad, Iran
e-mail: kianoosh.py@gmail.com

1 Introduction

Airplane wing performance has a substantial effect on not only the runway length, approach speed, climb rate, cargo capacity, and operation range but also the community noise and emission levels [1]. The wing performance is often degraded by flow separation, which strongly depends on the aerodynamic design of the airfoil profile. Furthermore, non-aerodynamic constraints are often in conflict with aerodynamic restrictions, and flow control is required to overcome such difficulties. Techniques that have been developed to manipulate the boundary layer, either to increase the lift or decrease the drag, and separation delay are classified under the general heading of flow control [2]. Flow control methods are divided into passive, which require no auxiliary power and no control loop, and active, which require energy expenditure. Passive techniques include geometric shaping, the use of vortex generators, and the placement of longitudinal

grooves or riblets on airfoil surfaces. Examples of active flow control methods include steady suction or blowing, unsteady suction or blowing, and the use of synthetic jets.

Over the past several decades, numerous surveys have been conducted on suction and blowing flow control approaches. Prandtl was the first scientist to employ boundary layer suction on a cylindrical surface for delaying flow separation. The earliest known experimental studies [3–5] on the boundary layer suction of wings were carried out in the late 1930s and 1940s, primarily in wind tunnels. Suction and blowing approaches have since emerged and been evaluated in a variety of experiments [6–9] to improve the efficiency and stability of lift systems. With the recent advances in computational facilities, computational fluid dynamics (CFD) is increasingly being used for investigating three-dimensional flow fields. Shan et al. [10] numerically studied the flow separation and transition around a NACA 0012 airfoil using the direct numerical simulation (DNS) method and captured details regarding flow separation, vortex shedding, and boundary layer reattachment. Moreover, several three-dimensional CFD studies [11–15] have been carried out to simplify the simulation of flow fields around airfoils by neglecting active or passive flow control techniques. In addition, flow control methods such as suction, blowing, and the use of synthetic jets have been investigated experimentally [16–19] over thick and NACA airfoils under different flow conditions. In these studies, the effects of control devices were considered on the lift and drag coefficients, mean pressure coefficients, separation and transition locations, and wake profiles.

Unfortunately, three-dimensional (3D) flow control surveys are severely limited. Deng et al. [20] examined blowing flow control via the DNS method to optimize the blowing jets. They studied the effects of different unsteady blowing jets on the surface at locations just before the separation points, and the separation bubble length was significantly reduced after unsteady blowing was applied. Brehm et al. [21] employed CFD methods to investigate flow fields around uncontrolled and controlled NACA 64_3-618 airfoils by blowing and suction through a slot using 3D Navier–Stokes simulations. They found that exploiting the hydrodynamic instability of the base flow made control more effective. You and Moin [22] performed a numerical large eddy simulation (LES) study of turbulent flow separation and evaluated the effectiveness of synthetic jets as a separation control technique. They demonstrated and confirmed that synthetic jet actuation effectively delays the onset of flow separation and significantly increases the lift coefficient. Recently, Bres et al. [23] performed a computational study on pulsed-blowing flow control of a semicircular planform wing. Overall, their results showed that the technique had good feasibility for industrial applications, particularly MAVs, and was effective at controlling separation.

Recently, there have been many studies on flow control approaches, particularly for two-dimensional (2D) flow fields [24–26]. However, 3D surveys of active/passive flow control techniques are severely limited owing to the convoluted flow conditions over wings. The flow over an airfoil is inherently complex and exhibits a variety of physical phenomena such as strong pressure gradients, flow separation, and the confluence of boundary layers and wakes. The flow over an airfoil is two-dimensional; in contrast, a finite wing is a three-dimensional body, so the flow over a finite wing is three-dimensional. Hence, the characteristics of a finite wing are not identical to the characteristics of its airfoil sections, so the numerical computations of flow over a finite wing are more challenging. The flow over a wing has additional parameters compared to its airfoil section, including the induced drag, downwash, and trailing vortex. Accordingly, the 3D simulation of a finite wing is highly complex and costly. This has apparently led to a lack of numerical surveys on 3D flow control. Therefore, the present study numerically investigated the influence of the suction flow control technique on a rectangular wing with a NACA 0012 section and optimization of the suction slot length. The computations incorporated a number of parameters: i.e., the jet length, momentum coefficient, and angle of attack at a Reynolds number of 5×10^5. The 3D simulation results were compared to experimental and numerical data for both controlled and uncontrolled cases; the effects of flow control on the lift and drag coefficients were examined, and the optimum length of the suction jet was determined.

2 Governing equations

The fluid flow was modeled as a three-dimensional, unsteady, turbulent, and viscous incompressible flow

with constant properties. The governing partial differential equations for the conservation of mass and momentum are as follows:

$$\frac{\partial \bar{u}_i}{\partial x_i} = 0 \tag{1}$$

$$\frac{\partial}{\partial x_j}(\bar{u}_i \bar{u}_j) = \frac{1}{\rho}\frac{\partial \bar{P}}{\partial x_i} + \frac{\partial}{\partial x_j}\left[\nu \frac{\partial \bar{u}_i}{\partial x_j} - \overline{u_i' u_j'}\right] \tag{2}$$

where ρ is the density, $\bar{P}$ is the mean pressure, ν is the kinematic viscosity, and $\bar{u}$ is the mean velocity. The Reynolds stress tensor $-\overline{u_i' u_j'}$ incorporates the effects of turbulent fluctuations. The Reynolds stresses were modeled via the Boussinesq approximation [27], where the deviatoric part is taken to be proportional to the strain rate tensor through the turbulent viscosity. The incompressible form of the Boussinesq approximation is

$$\overline{u_i' u_j'} = \nu_t \left(\frac{\partial \bar{u}_i}{\partial x_j} + \frac{\partial \bar{u}_j}{\partial x_i}\right) - \frac{2}{3} k \delta_{ij} \tag{3}$$

$$k = \frac{1}{2}\left(\overline{u'^2} + \overline{v'^2} + \overline{w'^2}\right) \tag{4}$$

In the above equation, ν_t is the turbulent viscosity, k is the average kinetic energy of the velocity fluctuations, and δ_{ij} is the Kronecker delta. In order to simulate the turbulent flow, eddy viscosity turbulent models such as algebraic or zero-equation models, one-equation models, and two-equation models employ the eddy or turbulent viscosity distribution rather than the Reynolds stress tensor.

The present computation used the Menter's shear stress transport two-equation model (k–ω SST) for the turbulence; this model provides excellent predictive capability for flows with separation. This model includes both k–ω and k–ε standard models, which improves the calculations of boundary layer flows with separation and removes the sensitivity of the k–ω model for external flows. The transport equations in Menter's shear stress model are as follows:

$$\frac{\partial}{\partial x_i}(\rho U_i k) = \tilde{P}_k - \beta^* \rho k \omega + \frac{\partial}{\partial x_i}\left[(\mu + \sigma_k \mu_t)\frac{\partial k}{\partial x_i}\right] \tag{5}$$

$$\frac{\partial}{\partial x_i}(\rho U_i \omega) = \alpha \rho S^2 - \beta \rho \omega^2 + \frac{\partial}{\partial x_i}\left[(\mu + \sigma_\omega \mu_t)\frac{\partial \omega}{\partial x_i}\right] + 2(1 - F_1)\rho \sigma_{w2}\frac{1}{\omega}\frac{\partial k}{\partial x_i}\frac{\partial \omega}{\partial x_i} \tag{6}$$

where F_1 is the blending function, S is the invariant measure of the strain rate, β^* is 0.09, and σ_{w2} is 0.856. The blending function is equal to zero away from the surface (k–ε model) and switches to unity inside the boundary layer (k–ω model). The production limiter $\tilde{P}_k$ is used in the SST model to prevent the buildup of turbulence in stagnant regions. All constants are computed by a blend of the corresponding constants for the k–ε and k–ω models via α, σ_k, σ_ω, etc. [28].

3 Numerical methodology

3.1 Wing geometry

All calculations were performed for a rectangular wing with a NACA 0012 airfoil section having a chord length of 1 m, as shown in Fig. 1. Since a rectangular wing was considered, the taper ratio was equal to 1. The aspect ratio is an important geometric property of a finite wing that varies according to the airplane performance and a predetermined cost. The aspect ratio is typically 4–12 for standard airplanes [29–31], and the most commonly applied aspect ratios are 4–6. Therefore, an aspect ratio of 4 was used in the present study; i.e., the wingspan was four times the length of the wing chord length (in rectangular wings, the tip chord length is equal to the root chord length). Owing to the symmetrical geometry of the wing, the symmetry condition was used in all cases to reduce the computation cost. Consequently, all of the figures show half of the wing in the Z direction.

3.2 Grid setup

A C-type zone with multizonal blocks was generated as a computational area, as shown in Fig. 2. The computational area was chosen to be large enough to prevent the outer boundary from affecting the near

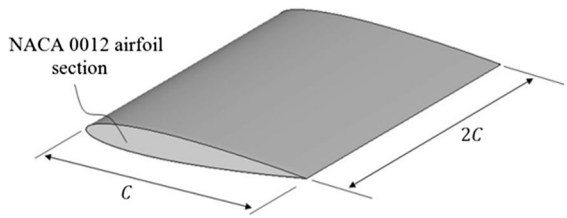

Fig. 1 Rectangular wing with NACA 0012 airfoil section

flow field around the airfoil. The grid extended from −4C upstream to 11C downstream, and the upper and lower boundaries extended 5C from the profile. Furthermore, the grid extended 4C in the spanwise direction, which was divided into two regions with lengths of 2C for each area along the lateral axis. The wing was located in the first region, and the fluid flow of air was in the next area (adjacent to the wing). Applying such a division allowed the use of fine-grid patches near the wing and in the regions of highly active flow since the most important physical phenomena occurred in this area: e.g., boundary layer separation, wakes, and vortexes. Moreover, the grid with multizonal blocks, total of 13 blocks, reduced the costs and allowed the capture of vital phenomena.

The inlet (left) and bottom boundaries were fixed with a uniform inlet velocity of $u_\infty = 7.3$ m/s, and the outer (right) and top boundary conditions were free stream boundaries that satisfied the Neumann condition. The symmetry condition was used for XY planes, as illustrated in Fig. 2. The no-slip boundary condition was used at solid surfaces, and the transpiration boundary condition was applied at the determined jet location to simulate suction. A low freestream turbulence level was used to match the wind tunnel characteristics, so the stream turbulence intensity was less than 0.1 %.

A structured grid was used in this investigation. The blocks around and beside the wing were the most

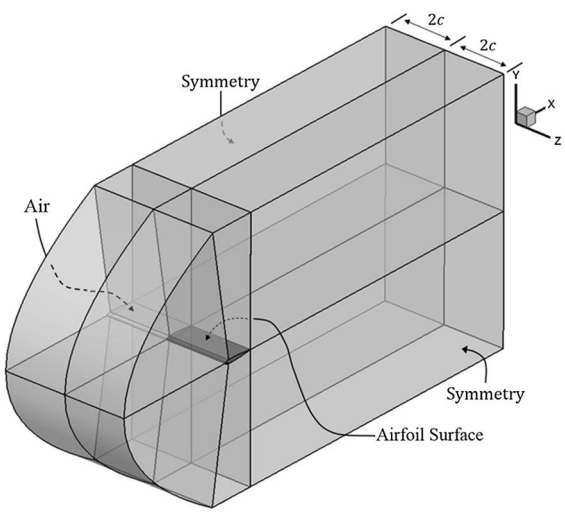

Fig. 2 C-type zone for NACA 0012 wing with multizonal blocks, 13 blocks in total, and symmetry boundary conditions for z = 0, −4 planes

sensitive computation areas, so the number of grid points in these blocks was most critical. In order to ensure grid independence, five sets of grids with increasing grid density were used to study lift and drag coefficients under a Reynolds number of 5×10^5, and angles of attack of 16° and 18° to determine the baseline conditions; the results are listed in Table 1. According to Table 1, the differences between sets 3 and 4 and between sets 4 and 5 were less than 1 %. To maintain grid-resolution consistency for different cases and with relatively high accuracy, the dense grid of set 4 was adopted for the current computation. Set 4 had about 1,700,000 cells, and the computation time was around 22 h using a computer with 20 processors for each case.

At angles of attack of less than 18°, even the coarse grid provided acceptable accuracy. Set 2 had approximately 625,000 cells, and increasing the grid density varied the lift and drag coefficients by negligible amounts of about 5 and 1 %, respectively. Nevertheless, the variations in the lift and drag coefficients were significant when the angle of attack was 18° or more. In this study, in order to simulate the boundary layer flow properly, the first layer grid near the wall satisfied the condition of y-plus <1.

3.3 Numerical method

The commercial RANS-based code FLUENT, which is based on a finite volume computational procedure, was used in this study. In the simulations, first- and second-order upwind discretization schemes were employed to discretize the convective terms in the momentum and turbulence equations. A first-order upwind discretization in space was used, and the resulting system of equations was then solved using the SIMPLE procedure until the convergence criterion of O(3) reduction for all dependent residuals was satisfied. The second-order upwind method was then applied to discretize the equations; following that, the equations were resolved through the SIMPLE method until precise convergence was achieved at O(6) for all dependent residuals. The results obtained from the first-order upwind method were used as the initial assumption for the second-order upwind method. The central difference scheme was also used for the diffusive terms, and the SIMPLE algorithm was applied for pressure–velocity coupling. The residuals in all simulations continued until the lift and drag

Table 1 Grid independence study for NACA 0012 wing at $Re = 5 \times 10^5$ and angles of attack of 16° and 18°

Number of cells	Angle of attack 16°		Angle of attack 18°	
	Lift coefficient	Drag coefficient	Lift coefficient	Drag coefficient
Set 1: 422,440	0.9283	0.1277	1.0349	0.1609
Set 2: 625,640	0.9177	0.1278	0.8954	0.1805
Set 3: 1,048,080	0.9022	0.127	0.8309	0.1821
Set 4: 1,673,720	0.8961	0.1268	0.7339	0.1945
Set 5: 2,299,360	0.8979	0.1268	0.7381	0.1956

coefficients reached full convergence. However, complete convergence occurred less frequently for small angles of attack, and the number of iterations rose as the angle of attack increased.

The present study used a Reynolds number of 5×10^5; consequently, a fully turbulent flow was reasonably assumed, and no transition was involved in the computations. This simulation employed parallel processing to allow different computational zones to be solved on different processors. The present study used a 20-core supercomputer (Intel Core i5-2500 K processor with 20 GB RAM and the Windows 7 64-bit operating system with service pack 1), which was supported by the Mechanical Engineering Department at Islamic Azad University, Mashhad Branch.

The computation results were compared with the 2D numerical simulation data of Yousefi et al. [24] and Huang et al. [26], and the experimental results of Jacobs et al. [32] and Critzos et al. [33], as shown in Fig. 3. All of these studies were performed at a Reynolds number of 5×10^5. As shown in the figure, the computation results agreed well with the experimental values of Jacobs et al. The highest recorded error for the lift and drag coefficients was less than 5 % when compared with the experimental values. However, both numerical works using 2D and 3D simulations showed that stalling occurred at an angle of attack of 14°, whereas the empirical measurements indicated that the NACA 0012 wing stalled at an angle of attack of 12°. The computational results of the lift and drag coefficients more closely agreed with the experimental data relative to other numerical works. For the lift coefficient, the present computation results were closer to the empirical measurements than those of Yousefi et al. [24] and

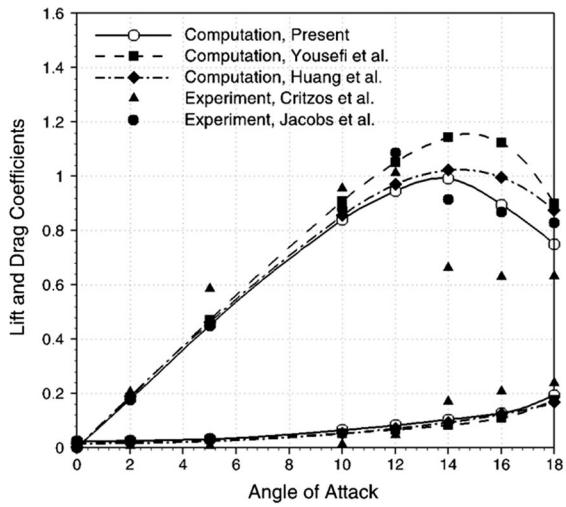

Fig. 3 Comparison between computation results, previous numerical data [24, 26], and experimental results [32, 33]

Huang et al. [26] by about 25 and 6 %, respectively, at the stall angle; they were 27 and 20 % closer, respectively, at an angle of attack of 18°. It can be seen from Fig. 3 and other studies [32, 34] that the experimental data in the literature vary widely, which implies a large amount of experimental uncertainty. This uncertainty can be attributed to several factors, such as different flow regimes, angles of attack, and airfoil geometries. In addition to the inherent complexity of turbulent regimes, the differences between the experimental and numerical simulation results for the airfoils and wings can be caused by other errors and difficulties on both the experimental and numerical sides. On the experimental side, installation errors for the wing model, disturbances to the measurement device, interference between the wind-tunnel wall and wing body,

and freestream turbulence can create errors in measurement. On the numerical simulation side, turbulence models, artificial viscosity, and grid density can develop computational inaccuracies. Despite these challenges, the present computation eliminated the limitations of two-dimensional simulation.

3.4 Parameter selection

The perpendicular suction at the leading edge over a rectangular wing with a NACA 0012 airfoil profile was computationally investigated. Figure 4 shows the suction jet location (L_j), jet width (h), and jet length (b_s) for the NACA 0012 wing. According to previous studies [6, 24], the optimum width of the suction area is about 2.5 % of the chord length, and the aerodynamic characteristics do not increase significantly beyond this size. Consequently, the suction jet width was fixed to 2.5 % of the chord length for all computations. The perpendicular suction at the leading edge for 0.075–0.125 of the chord length was better than other suction situations at increasing lift [26]; therefore, the jet location was set to 10 % of the chord length from the leading edge. The suction jet length (b_s) was varied from 0.25 to 2 of the chord length. The jet amplitude, or the jet velocity to the freestream velocity ratio, was set to 0.5. Furthermore, angles of attack of 12°, 14°, 16°, and 18° were used for analysis. The jet entrance velocity is defined as

$$u = u_j \cdot \cos(\theta + \beta) \tag{7}$$

$$v = u_j \cdot \sin(\theta + \beta) \tag{8}$$

where β is the angle between the freestream velocity direction and local jet surface, and θ is also the angle between the local jet surface and jet output velocity direction. A negative θ represents a suction condition, and a positive θ indicates a blowing condition. For perpendicular suction, θ is −90°. The effects of the suction jet were characterized through an important dimensionless parameter, the momentum coefficient [35, 36]:

$$C_\mu = \frac{M_j}{M_\infty} = \frac{\rho A_j u_j^2}{\rho A_\infty u_\infty^2} \tag{9}$$

The wing surface area and suction jet area are defined as $A_\infty = c \times b$ and $A_j = h \times b_s$, respectively, where b is the wingspan, h is the suction width, and b_s refers to the suction length. By substituting the above relations into Eq. 10, the jet momentum coefficient is represented as

$$C_\mu = \frac{\rho(h \times b_s)u_j^2}{\rho(c \times b)u_\infty^2} = \frac{b_s}{b}\frac{h}{c}\left(\frac{u_j}{u_\infty}\right)^2 \tag{10}$$

Working with dimensionless parameters is more convenient; therefore, the following dimensionless variables were defined: jet amplitude (A), jet width (H), and jet length (B).

$$A = \frac{u_j}{u_\infty} \tag{11}$$

$$H = \frac{h}{C} \tag{12}$$

$$B = \frac{b_s}{b} \tag{13}$$

All of the above parameters change over the range $0 < A, H, B < 1.0$. The jet momentum coefficient is ultimately expressed as

$$C_\mu = BHA^2 \tag{14}$$

As shown in Eq. 14, the jet momentum coefficient depends on the three dimensionless parameters A, H and B. The jet amplitude and jet width were assumed to be 0.5 and 0.025, respectively. Consequently, by changing the jet length to 0.25–2 of the chord length, the jet momentum coefficient varied between 0.00078 and 0.00625. Thus, the momentum coefficient covered a greater range than those used in previous experimental and numerical investigations.

One innovation of this study was that the suction over the wing was incomplete for jet lengths of less than 2C, and the whole wingspan area was not covered by suction slots. This incomplete suction area

Fig. 4 NACA 0012 wing with suction slot

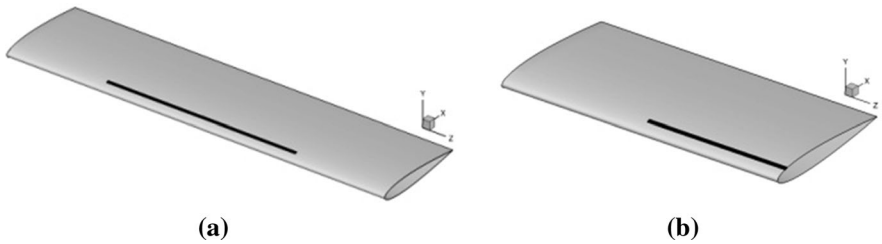

Fig. 5 NACA 0012 wing with center suction slot: **a** full view and **b** symmetric view

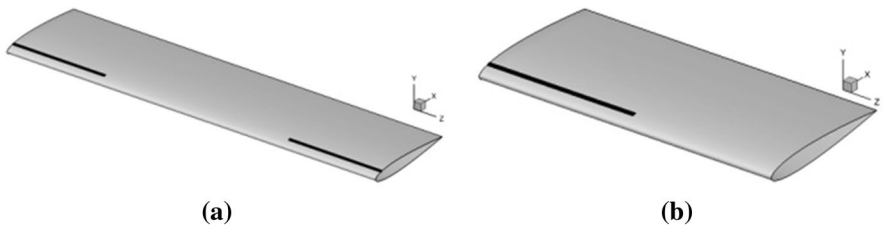

Fig. 6 NACA 0012 wing with tip suction slot: **a** full view and **b** symmetric view

provided two different distributions of suction slots over the wing. Hence, suction can occur from the center of the wing (i.e., center suction) or from the wing tip (i.e., tip suction); these are shown in Figs. 5 and 6, respectively.

4 Results and discussion

4.1 Center suction

The obtained analysis results for the perpendicular suction over the NACA 0012 wing are given below. First, the effect of the jet length on the aerodynamic characteristics was investigated for the center suction. Figures 7, 8 and 9 show the changes in the lift coefficient, drag coefficient, and lift-to-drag ratio versus the angle of attack for different jet lengths of the center suction. Increasing the suction jet length increased the lift coefficient and decreased the drag coefficient, which increased the lift-to-drag ratio. This improvement in the lift-to-drag ratio was negligible for angles of attack of less than 14°, but the suction flow control had a pivotal impact beyond the stall angle, particularly at angles of attack of 18° and above. When suction flow control was applied to the NACA 0012 wing, the lift-to-drag ratio reached its maximum when the jet length was equal to the wingspan. At this point, the momentum coefficient was 0.00625. In this situation, the center and tip suctions were the same: the lift-to-drag ratio increased by 130 % as the lift coefficient increased by 60 % and the drag coefficient decreased by 30 %. Using jet lengths of 0.25, 0.5, 1, 1.5, and 1.75 of the chord length increased the lift-to-drag ratio by 2, 6, 51, 85, and 122 %, respectively, at an angle of attack of 18°.

As shown in Figs. 10 and 11, the velocity contours and streamline patterns of different jet lengths were compared with the baseline case for further exploration. The figures plot the results for jet lengths of 0.5, 1.0, and 1.5C against the no-control case under a jet amplitude of 0.5, jet location of 0.1 %, and angle of attack of 18°. In all cases, the streamline patterns clearly demonstrated smaller wakes on the wing than the baseline case without a jet implementation. When the jet length was increased, the separation bubble was effectively delayed; hence, the separation bubbles and wakes were almost entirely eliminated for suction jet lengths of 1C and above, especially at 1.75C. Therefore, among the tested jet lengths, a suction jet length of about 1.75 of the chord length produces the most positive effect on aerodynamic features to manipulate the boundary layer in order to increase the lift-to-drag ratio and remove undesirable vortexes. Increasing the jet length makes the flow over the wing more stable; however, the difference when the jet length was greater than the chord length was insignificant, particularly for jet lengths of 1.75 and 2 of the chord length.

Unfortunately, there has been no experimental and 3D numerical work on suction flow control techniques for this airfoil under the flow conditions used in the current computation; thus, only 2D simulation was

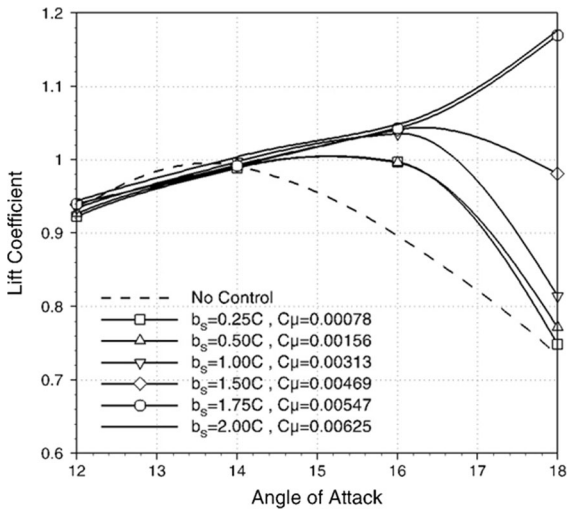

Fig. 7 Effect of suction jet length on lift coefficient of NACA 0012 wing for center suction

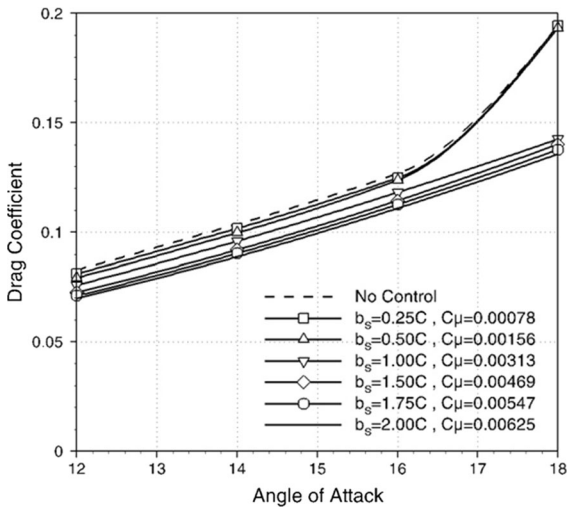

Fig. 8 Effect of suction jet length on drag coefficient of NACA 0012 wing for center suction

available to validate the controlled situation. In order to provide an accurate comparison with the computational data, the ratio of the controlled lift coefficient C_L to the uncontrolled or natural lift coefficient $C_{L,B}$ of the present three-dimensional simulation was compared with other two-dimensional numerical results under a jet location of 0.1 %, jet amplitude of 0.5, momentum coefficient of 0.00625, and angle of attack of 18°. Yousefi et al. [24] and Huang et al. [26] had $C_L/C_{L,B}$ ratios of 1.75 and 1.55, respectively, whereas the present finite wing simulation had a ratio of 1.60.

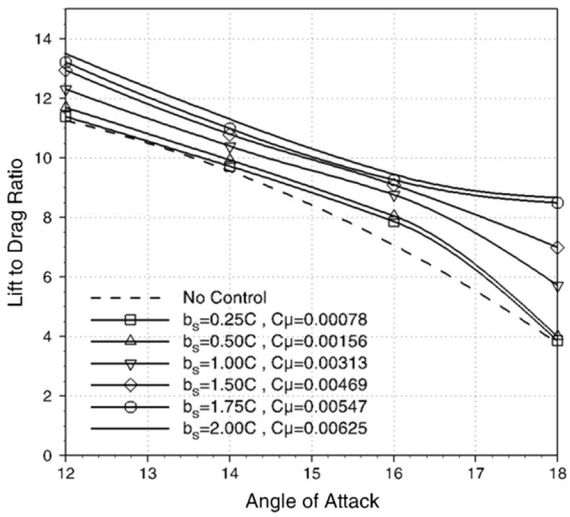

Fig. 9 Effect of suction jet length on lift-to-drag ratio of NACA 0012 wing for center suction

4.2 Tip suction

Figures 12, 13 and 14 show the effects of the changes in jet length on the lift coefficient, drag coefficient, and lift-to-drag ratio. Similar to the center suction, increasing the jet length for the tip suction caused the lift coefficient to rise and the drag coefficient to fall, which improved the lift-to-drag ratio. The maximum increase in the aerodynamic characteristics, particularly the lift-to-drag ratio, again occurred when the jet length was 1.75 of the chord length at 43 %; the lift coefficient increased 25 %, whereas the drag coefficient decreased 17 %. The lift-to-drag ratio increased by 9, 12, 16, and 25 % for jet lengths of 0.25, 0.5, 1.0, and 1.5 of the chord length, respectively. When the jet length was less than the chord length, the tip suction was better at increasing the aerodynamic features compared to the center suction. For example, when the jet length was 0.5 of the chord length, the center and tip suctions increased the lift-to-drag ratio by 6 and 12 %, respectively. Thus, the tip suction increased the lift-to-drag ratio by twofold compared to the center suction. Figures 15 and 16 show the changes in the velocity contours and flow patterns due to variations in the jet length for the tip suction at an angle of attack of 18°. Lengthening the jet clearly had a positive impact. The flow pattern at a jet length of 0.25 of the chord length was essentially the same as

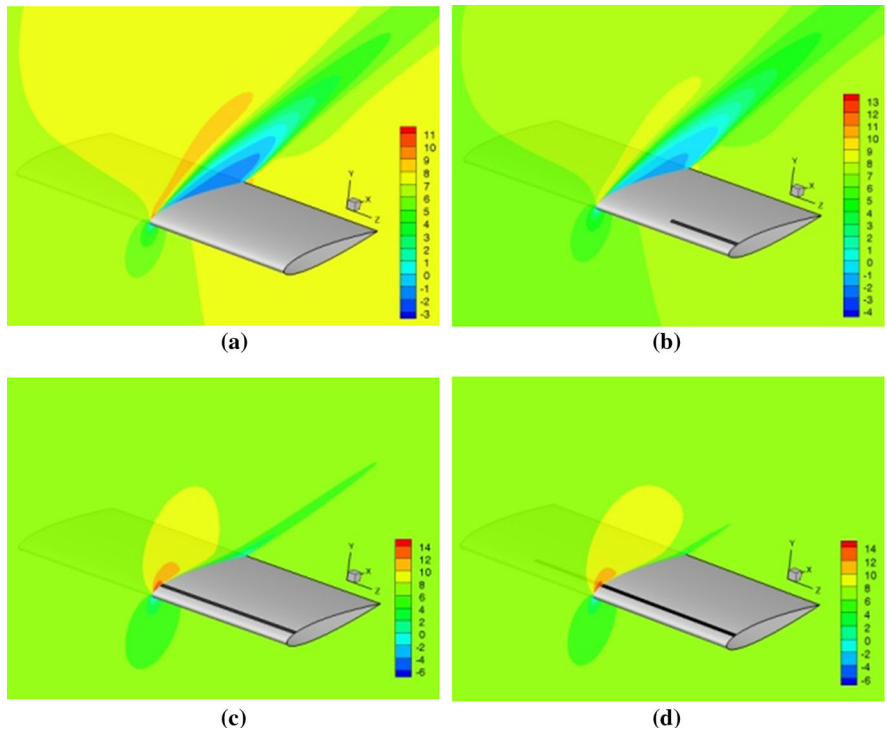

Fig. 10 Velocity contour at $Z = -1$ plane and angle of attack of 18° for center suction: **a** no control, **b** $b_s = 0.5$ C, **c** $b_s = 1.0$ C, and **d** $b_s = 1.5$

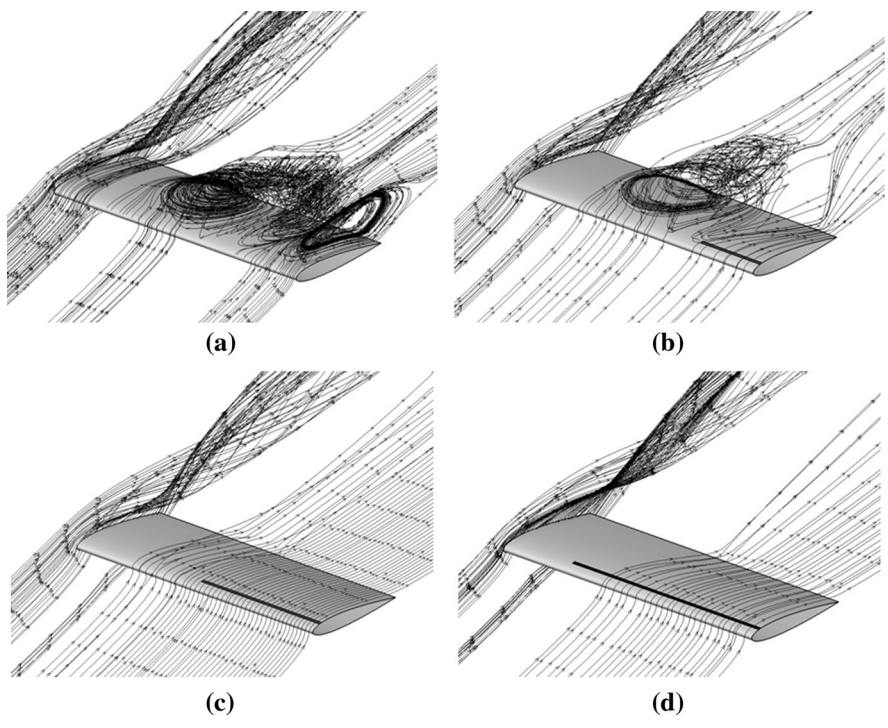

Fig. 11 Effect of suction jet length on streamlines over finite wing at angle of attack of 18° for center suction: **a** no control, **b** $b_s = 0.5$C, **c** $b_s = 1.0$C, and **d** $b_s = 1.5$C

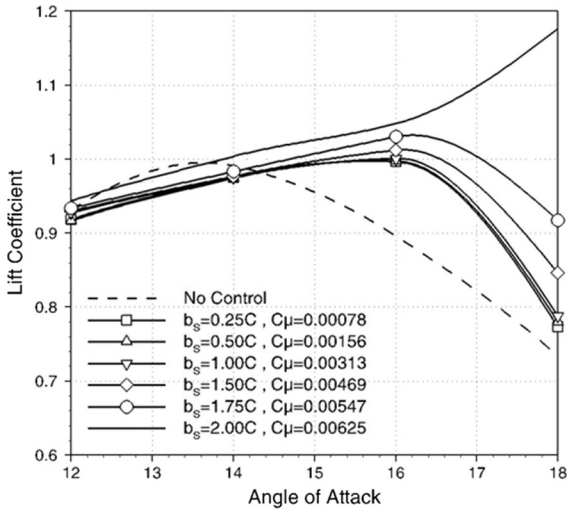

Fig. 12 Effect of suction jet length on lift coefficient of NACA 0012 wing for tip suction

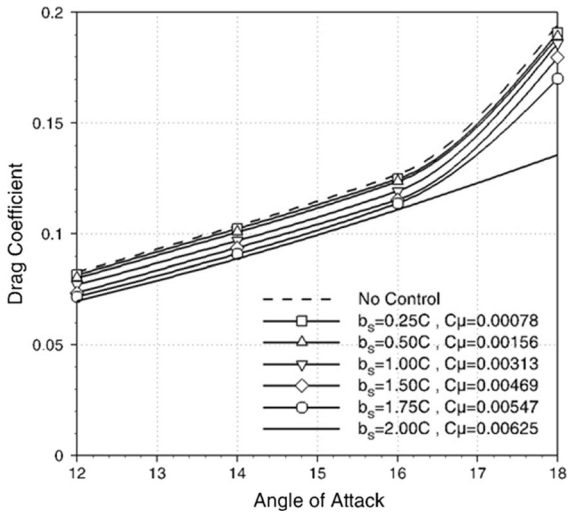

Fig. 13 Effect of suction jet length on drag coefficient of NACA 0012 wing for tip suction

the baseline case, and fewer wakes were eliminated, in contrast to the center suction in similar situations, even when the jet was very long.

Three factors affect the lift and drag: changes in the upper surface pressure; variations in shear stress near the surface, and changes in the overall circulation about the wing. These were extensively examined in several studies [6, 26] that determined the pivotal driving factors that cause changes in the lift and drag coefficients.

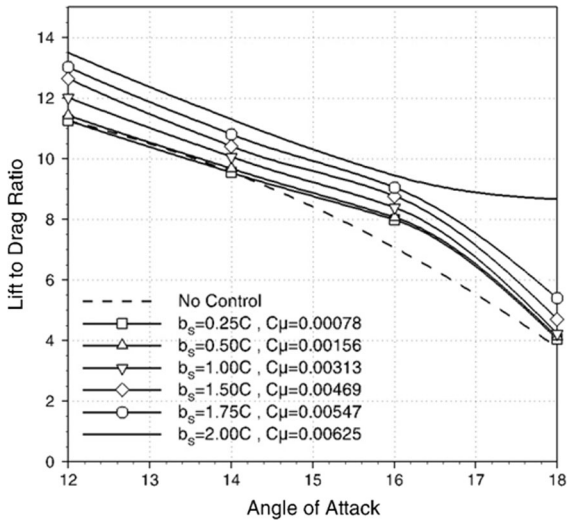

Fig. 14 Effect of suction jet length on lift-to-drag ratio of NACA 0012 wing for tip suction

4.3 Comparison of center and tip suctions

The differences between the center and tip suctions are presented below. Figures 17, 18, 19, 20 and 21 compare the lift-to-drag ratios of the center and tip suctions for different jet lengths at angles of attack of 12°–18°. The results showed that center suction was the better choice in more cases. Increasing the suction jet length made center suction more effective, and the lift-to-drag ratio increased more with center suction than with tip suction. For center suction, when the jet length was 0.25 of the chord length and the angle of attack was 18°, the lift coefficient increased by 2 %, and the drag coefficient remained roughly constant. With tip suction, the lift coefficient increased 5 %, and the drag coefficient decreased 2 %. However when the suction jet length was 1.75 of the chord length with the same angle of attack, the lift coefficient increased by 58 and 25 % and the drag coefficient declined by 28 and 12.5 % with center and tip suctions, respectively. Figures 11 and 16 clearly show that the separation was most effectively delayed when center suction was applied, and the wake profiles were much smaller compared to the other case. Center suction eliminated more vortexes since most of the wakes were concentrated at the center of the wing when there was no control. Vortexes naturally start from the wing tip and develop toward the center.

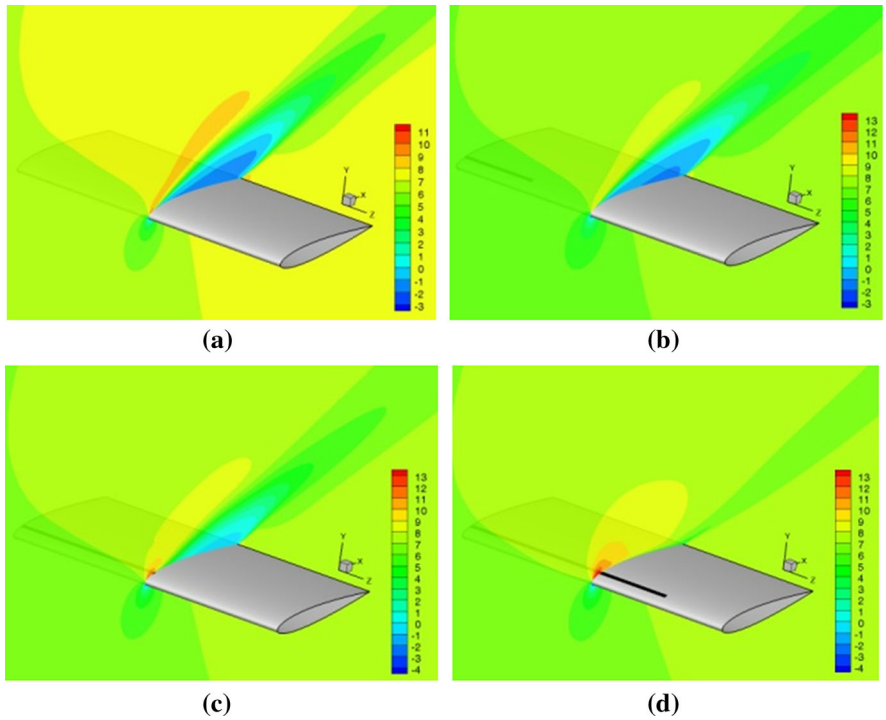

Fig. 15 Velocity contour at $Z = -1$ plane and angle of attack of 18° for tip suction: **a** no control, **b** $b_s = 0.5C$, **c** $b_s = 1.0C$, and **d** $b_s = 1.5C$

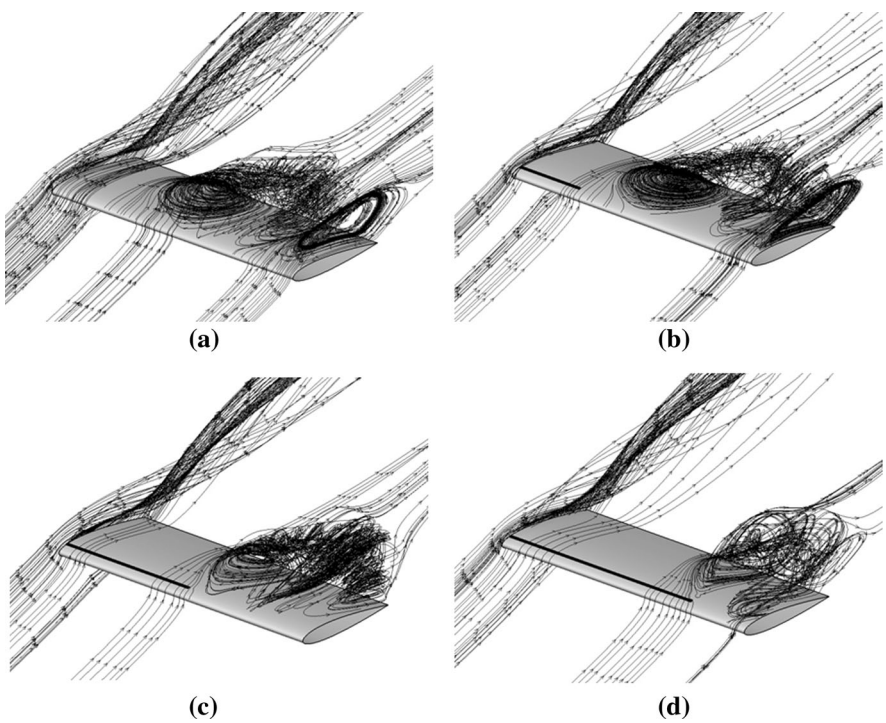

Fig. 16 Effect of suction jet length on streamlines over finite wing at angle of attack of 18° for tip suction: **a** no control, **b** $b_s = 0.5C$, **c** $b_s = 1.0$ C, and **d** $b_s = 1.5C$

Thus, when the suction jet length was $0 < B \leq 0.5$, tip suction was the best choice, and when the suction jet length was $0.5 < B \leq 1.0$, center suction was the most effective choice. In other words, when the length of the suction area is less than half of the wingspan, tip suction is more suitable than center suction, and when

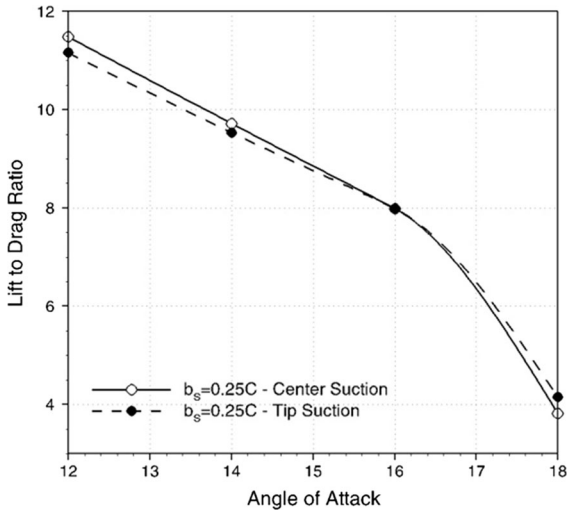

Fig. 17 Comparison of lift-to-drag ratios for center and tip suctions with jet length of 0.25C

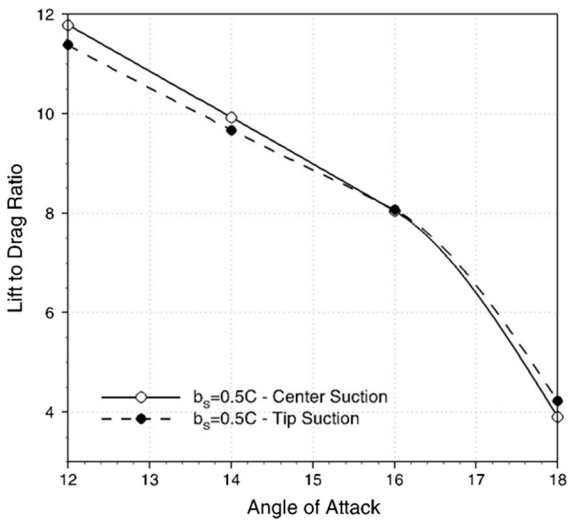

Fig. 18 Comparison of lift-to-drag ratios for center and tip suctions with jet length of 0.5C

the length of the suction area is greater than half of the wingspan, center suction is better. The optimum jet length for perpendicular suction of a NACA 0012 wing is ultimately expressed as follows:

$$\begin{cases} 0 < B \leq 0.5 & \text{Tip Suction} \\ 0.5 < B \leq 1 & \text{Center Suction} \end{cases} \quad (15)$$

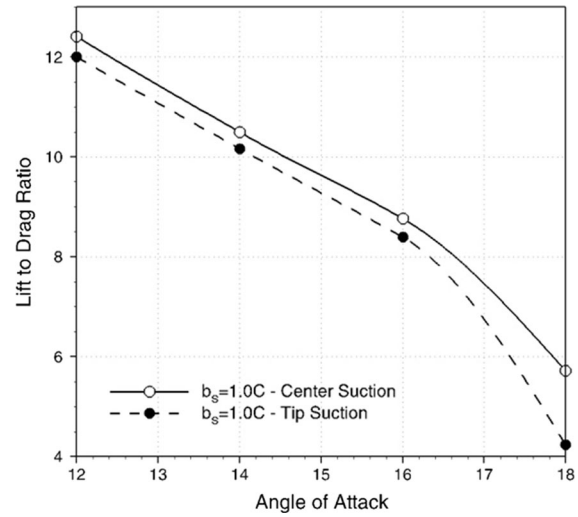

Fig. 19 Comparison of lift-to-drag ratios for center and tip suctions with jet length of 1.0C

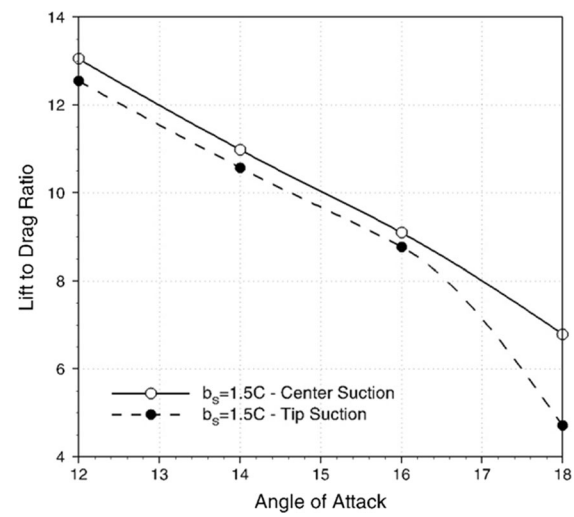

Fig. 20 Comparison of lift-to-drag ratios for center and tip suctions with jet length of 1.5C

5 Conclusion

This study evaluated the effects of suction flow control on a rectangular wing with a NACA 0012 airfoil section at a Reynolds number of 5×10^5 and different angles of attack. The suction jet length was varied over a wide range to determine the optimum jet length. This

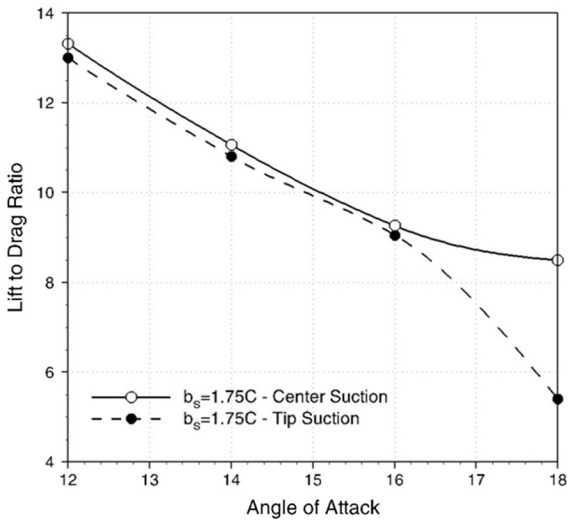

Fig. 21 Comparison of lift-to-drag ratios for center and tip suctions with jet length of 1.75C

three-dimensional study obtained interesting and valuable results, which are summarized below.

A longer suction jet unsurprisingly had a larger impact on the flow field around the wing. When the jet length was increased, the lift coefficient rose and the drag coefficient fell, which improved the lift-to-drag ratio for both center and tip suctions. The center suction became more effective when the jet was lengthened, and the lift-to-drag ratio improved more with center suction than with tip suction. When the jet was short, tip suction produced a higher lift-to-drag ratio. The lift-to-drag ratio rose by 2 and 122 % for center suction jet lengths of 0.25 and 1.75 of the chord length, respectively. It increased by 9 and 43 % for tip suction jet lengths of 0.25 and 1.75 of the chord length, respectively. Furthermore, increasing the jet length was effective at delaying the separation bubbles and vortexes, particularly with center suction; consequently, the separation bubbles and wakes were almost entirely eliminated by using center suction.

In conclusion, tip suction is a better choice when the suction jet length is $0 < B \leq 0.5$, whereas center suction is better when the suction jet length B is between 0.5 and 1. In other words, tip suction is better when the jet length is less than half of the wingspan, while center suction is better when it is greater than half of the wingspan.

Acknowledgments The authors thank Dr. Mehrdad Jabbarzadeh, Dr. Majid Vafaei Jahan, and Mr. Soheil Namvar for providing vital resources for the supercomputer cluster. We also thank Dr. Behrooz Zafarmand for his valuable suggestions during the planning and development of this research.

References

1. Thibert JJ, Reneaux J, Moens F, Priest J (1995) ONERA activities on high lift devices for transport aircraft. Aeronaut J 99:395–411
2. Hazen DC (1968) Boundary layer control. J Fluid Mech 29:200–208
3. Richards EJ, Burge CH (1943) An airfoil designed to give laminar flow over the surface with boundary layer suction. Aeronautical Research Council, R&M 2263
4. Walker SW, Raymer WG (1946) Wind tunnel test on the 30 percent symmetrical griffith aerofoil with ejection of air. Aeronautical Research Council R&M 2475
5. Braslow AL (1999) A history of suction type laminar flow control with emphasis on flight research, NASA History Division, Monograph in Aerospace History
6. Dannenberg RE, Weiberg JA (1952) Section characteristics of a 10.5 % thick airfoil with area suction as affected by chordwise distribution of permeability, NACA technical note 2847
7. Dannenberg RE, Weiberg JA (1954) Section characteristics of an NACA0006 airfoil with area suction near the leading edge, NACA technical note 3285
8. Howe HJ, Neumann BJ (1982) An experimental evaluation of a low propulsive power discrete suction concept applied to an axisymmetric vehicle, David W. Taylor Naval Ship R&D Center TM 16-82/02
9. Dirlik S, Kimmel K, Sekelsky A, Slomski J (1992) Experimental evaluation of a 50-percent thick airfoil with blowing and suction boundary layer control, AIAA Paper No. AIAA-92-4500
10. Shan H, Jiang L, Liu C (2005) Direct numerical simulation of flow separation around a NACA 0012 Airfoil. Comput Fluids 34(9):1096–1114
11. Hoarau Y, Faghani D, Braza M, Perrin R, Anne-Archard D, Ruiz D (2003) Direct numerical simulation of the three-dimensional transition to turbulence in the incompressible flow around a wing. Flow Turbul Combust 71(1–4):119–132
12. Bourdet S, Bouhadji A, Braza M, Thiele F (2003) Direct numerical simulation of the three-dimensional transition to turbulence in the transonic flow around a wing. Flow Turbul Combust 71(1–4):203–220
13. Martinat G, Braza M, Hoarau Y, Harran G (2008) Turbulence modeling of the flow past a pitching NACA 0012 Airfoil at 10^5 and 10^6 reynolds numbers. J Fluids Struct 24(8):1294–1303
14. Uranga A, Persson P, Drela M. Peraire J (2009) Implicit large eddy simulation of transitional flows over airfoils and wings. In: 19th AIAA computational fluid dynamics, AIAA 2009-4131, San Antonio, Texas
15. Im HS, Zha GC (2011) Delayed detached eddy simulation of a stall flow over NACA0012 airfoil using high order schemes. In: 49th AIAA aerospace sciences meeting

including the new horizons forum and aerospace exposition, AIAA 2011-1297, Orlando, Florida
16. Gilarranz JL, Traub LW, Rediniotis OK (2005) A new class of synthetic jet actuators—part II: application to flow separation control. ASME J Fluids Eng 127(2):377–387
17. Timor I, Ben-Hamou E, Guy Y, Seifert A (2007) Maneuvering aspects and 3D effects of active airfoil flow control. Flow Turbul Combust 78(3–4):429–443
18. Troshin V, Seifert A (2013) Performance recovery of a thick turbulent airfoil using a distributed closed-loop flow control system. Exp Fluids 54(1), Article 1443
19. Buchmann NA, Atkinson C, Soria J (2013) Influence of ZNMF jet flow control on the spatio-temporal flow structure over a NACA-0015 airfoil. Exp Fluids 54(3), Article 1485
20. Deng S, Jiang L, Liu C (2007) DNS for flow separation control around an airfoil by pulsed jets. Comput Fluids 36(6):1040–1060
21. Brehm C, Mack S, Gross A, Fasel HF (2008) Investigations of an airfoil at low reynolds number conditions. In: 4th flow control conference, AIAA 2008-3765, Seattle, Washington
22. You D, Moin P (2008) Active control of flow separation over an airfoil using synthetic jets. J Fluids Struct 24(8):1349–1357
23. Bres GA, Williams DR, Colonius T (2010) Numerical simulations of natural and actuated flow over a 3D, low-aspect-ratio airfoil. In: 40th fluid dynamics conference and exhibit, AIAA 2010-4713, Chicago, Illinois
24. Yousefi K, Saleh R, Zahedi P (2014) Numerical study of blowing and suction slot geometry optimization on NACA 0012 Airfoil. J Mech Sci Technol 28(4):1297–1310
25. Yousefi K, Saleh R (2014) The effects of trailing edge blowing on aerodynamic characteristics of the NACA0012 airfoil and optimization of the blowing slot geometry. J Theor Appl Mech 52(1):165–179
26. Huang L, Huang PG, LeBeau RP (2004) Numerical study of blowing and suction control mechanism on NACA0012 Airfoil. J Aircr 41(5):1005–1013
27. Alfonsi G (2009) Reynolds-averaged navier-stokes equations for turbulence modeling. Appl Mech Rev 62(4):040802
28. Menter FR, Kuntz M, Langtry R (2003) Ten years of industrial experience with the SST turbulence model. In: Proceedings of 4th international symposium on turbulence, heat and mass transfer, Turkey, pp 625–632
29. Hoarau Y, Braza M, Ventikos Y, Faghani D, Tzabiras G (2003) Organized modes and three-dimensional transition to turbulence in the incompressible flow around a NACA 0012 wing. J Fluids Mech 496:63–72
30. Marsden O, Bogey C, Bailly C (2006) Direct noise computation around a 3D NACA 0012 Airfoil. In: 27th AIAA aeroacoustics conference, AIAA 2006–2503, Massachusetts
31. Spentzos A, Barakos G, Badcock K, Ruchards B, Wernert P, Schreck S, Raffei M (2004) CFD investigation of 2D and 3D dynamic stall. In: AHS 4th decennial specialist's conference on aeromechanics, San Fransisco, California
32. Jacobs E, Sherman A (1937) Airfoil section characteristics as affected by variations of the reynolds number, NACA report no. 586–231
33. Critzos CC, Heyson HH, Boswinkle W (1955) Aerodynamics characteristics of NACA0012 airfoil section at angle of attacks from 0° to 180°, NACA technical note 3361
34. Mc Croskey WJ (1987) A critical assessment of wind tunnel results for the NACA 0012 Airfoil", NASA TM 100019
35. Buresti G (2009) Notes on the role of viscosity, vorticity and dissipation in incompressible flows. Meccanica 44(4):469–487
36. Graziani G, Bassanini P (2002) Unsteady viscous flows about bodies: vorticity release and forces. Meccanica 37(3):283–303